Probe of bending motion following the $1s^{-1}\pi^*$ excitation of N_2O

M. Machida
Department of Materials Science, Himeji Institute of Technology, Kamigori, Hyogo 678-1297, Japan

M. Lavollée
LURE, Batiment 209d, Centre Universitaire Paris-Sud, F-91898, Orsay Cedex, France

J. Randrianjafisoa
L. P. M. R., BP 141, Université d' Antananarivo, Madagascar

G. Laurent
Centre Interdisciplinaire de Recherches Ions Lasers, 14070 CAEN Cedex 5, France

M. Nagoshi
Department of Materials Science, Himeji Institute of Technology, Kamigori, Hyogo 678-1297, Japan

K. Okada
Department of Chemistry, Hiroshima University, Higashi-Hiroshima 739-8526, Japan

I. Koyano
Department of Materials Science, Himeji Institute of Technology, Kamigori, Hyogo 678-1297, Japan

N. Saito[a)]
National Metrology Institute of Japan, AIST, Tsukuba 305-8568, Japan

(Received 3 December 2002; accepted 24 November 2003)

The doubly degenerate core-excited Π state of N_2O splits into two due to the static Renner–Teller effect. The lower state, A_1, has a bent stable geometry and the molecule excited to this state starts to deform itself toward this bent geometry. To probe the effect of the potential energy surfaces of the core-excited A_1 states on the nuclear motion, we measure the momenta of the three atomic ions in coincidence by means of the ion momentum imaging technique. We find that the potential energy surface affects the molecular deformation significantly. N_2O in the terminal $N\,1s^{-1}3\pi A_1$ excited state is observed to be bent more than that in the central $N\,1s^{-1}3\pi A_1$ excited state. This means that N_2O in the terminal $N\,1s^{-1}3\pi A_1$ excited state bends faster than that in the central $N\,1s^{-1}3\pi A_1$ excited state. When the excitation energy is decreased within the $1s^{-1}3\pi$ resonances, the nuclear motion in the A_1 states becomes faster. This is interpreted by the notion that the excitation occurs onto the steeper slope part of the potential energy surface of the excited state for the lower excitation energy. The branching ratio of the A_1 excitation increases with the decrease in the excitation energy.
 [DOI: 10.1063/1.1641783]

I. INTRODUCTION

Nuclear motion plays an important role in the decay process of core excited states: although the core-hole lifetime is in the order of femtoseconds this motion can take place before the molecule deexcites through Auger transitions and dissociates into fragments, changing the expected kinetic energy distributions between these fragments[1–8] and even opening sometimes new decay channels unreachable in the initial geometry of the neutral molecule.[9]

This motion occurs when the stable geometry of the core-excited molecule is different from that of the ground state, which is often the case. For example, when a $C\,1s$ electron in a linear molecule CO_2 is promoted to the lowest unoccupied molecular orbital $2\pi_u$, the stable geometry of the core-excited $C\,1s^{-1}2\pi_u$ state is expected to be bent because the excited CO_2 molecule can be approximated, in the equivalent-core model, to the bent ground state of the molecule NO_2.[10–14] In our previous reports[15,16] we have demonstrated that the structural change from linear to bent geometry indeed occurs as a result of the $C\,1s\rightarrow 2\pi_u$ excitation, just as predicted by the $(Z+1)$ equivalent-core model, by probing the molecular geometry by means of the triple-ion-coincidence momentum imaging technique.

The $1s^{-1}\pi^*$ core-excited states of linear triatomic molecules such as CO_2, N_2O, OCS, and CS_2 are doubly degenerate.[13,17] These doubly degenerate core-excited states split into two states along the nontotally symmetric bending coordinate Q_2 due to vibronic coupling via the Q_2 mode, referred to as static Renner–Teller (RT) effect.[10–16,18–20] The lower branch of the RT pair states has a stable bent geometry. This bent state has an electron in the π orbital that lies in the plane defined by the bending motion of the molecule (in-plane, A_1 in C_{2v}). The upper branch, on the other hand, remains linear. This linear state has an electron in the π orbital that lies perpendicularly to that plane (out-of-plane, B_1 in C_{2v}). In our previous reports[15,16] we proved that the

a)Author to whom correspondence should be addressed. Electronic mail: norio.saito@aist.go.jp

core-excited CO_2 molecules in the in-plane A_1 state and the out-of-plane B_1 state are bent and linear, respectively. We also found that C $1s$ excited CO_2 is more bent than O $1s$ exited CO_2. This is mainly due to longer lifetime of the C $1s$ hole than that of the O $1s$ hole.

The N_2O molecule has two nitrogen atoms in different sites, i.e., center (Nc) and terminal (Nt). The lifetime of nitrogen core holes is not expected to depend on the site. Therefore we can derive the effect of the core-excited potential energy surfaces on the nuclear motion. Also we can compare the nuclear motions between the Nt $1s$ and O $1s$ core-excited states. There are limited works that predict the nuclear motion in the core-excited states of N_2O molecules.[21,22] LeBrun *et al.*[21] measured photoelectron-photoion-photoion coincidence spectra and the maximum kinetic energies of fragment ions from the Nt $1s^{-1}3\pi$ state and from the Nc $1s^{-1}3\pi$ state. The kinetic energies of the Nc^+ fragment ions produced by the Nt excitation are higher than those produced by the Nc excitation, which suggests that the Nt $1s$ excited N_2O molecules are more bent than the Nc $1s$ excited molecules. Adachi *et al.*[22] measured angle-resolved photoion-photoion coincidence spectra in the Nc and Nt core-excited states, with the result that the molecule in the Nc $1s^{-1}3\pi$ excited state is more bent than that in the Nt $1s^{-1}3\pi$ excited state. The stable bond angles for the Nt and Nc $1s^{-1}3\pi$ states were calculated to be 136° and 114° by the *ab initio* self-consistent field calculation,[17] respectively. From this fact, the molecule in the Nc $1s^{-1}3\pi$ state seems to be more bent. On the other hand, we calculate using the Hartree–Fock approximation that the potential depths of the Nt and Nc $1s^{-1}3\pi$ excited states at their equilibrium bond length are 1.63 and 0.46 eV, respectively, which suggests that the molecule in the Nt $1s^{-1}3\pi$ excited state should have faster bending motion than that in the Nc $1s^{-1}3\pi$ excited state, resulting that the molecule in the Nt $1s^{-1}3\pi$ excited state is more bent in the short lifetime of a core hole.

In the present paper we probe the bent and linear geometries of the core-excited RT pair states A_1 and B_1 of the N_2O core-excited states and show the potential energy surface dependence of the nuclear motion in the A_1 states. We employ the triple-ion-coincidence momentum imaging technique as in the preceding work.[15,16,23] This technique is based on the measurements of time-of-flight for all fragment ions using a position-sensitive detector and allows one to extract the complete information about the linear momentum (p_x, p_y, p_z) for each fragment ion. We probe the molecular geometry through the momenta of the three ions dissociated from the triply charged triatomic molecular ions. This is a weak channel, resulting in small branching ratio for the creation of the triply charged parent ion. These multiply charged parent ions have high internal energy and break up very rapidly due to Coulomb explosion. The vector correlation among the linear momenta of the fragment ions reflects the conformation of the core-excited molecule at the time when the Auger decay takes place because the properties of the excited state are independent of the decay channels. We assume that the bond breaking of the triple-ionized triatomic molecular ion is simultaneous and the axial-recoil approximation[24,25] is valid. These assumptions are reasonable for the dominant symmetric three-body break-up channels of the triple-ionized triatomic molecular ions.[15,23]

II. EXPERIMENT

The main experiments reported here are carried out on beamline SA22 at Super-ACO, some preliminary experiments being performed on the *c* branch of the soft x-ray photo-chemistry beamline 27SU at SPring-8.[26] The photon energy band passes employed are ~80 meV for N $1s$ excitation and ~100 meV for O $1s$ excitation. The experimental setups and procedures are given in the previous papers.[15,16,23] Briefly, three fragment ions N^+, N^+, and O^+ produced from a triply charged parent molecular ion N_2O^{3+} are detected in coincidence by use of a time-of-flight (TOF) mass spectrometer equipped with a multihit position-sensitive detector which consists of microchannel plates and a position-sensitive anode. The position-sensitive anode is homemade multianodes for the experiments at Super-ACO[23] and a delay-line anode (Roentdek HEX80[27]) for the preliminary experiments at SPring-8. The TOF axis is fixed in the direction perpendicular to both the photon beam direction and *E*. A beam of the sample gas N_2O is introduced into the ionization point and crossed with the photon beam. The sample gas of $^{14}N^{14}NO$ is used for the preliminary experiments at SPring-8. In this case, when N_2O molecules are bent to less than 120°, we find that it is impossible to distinguish the terminal Nt^+ ion from the central Nc^+ ion. Therefore we use isotopomer $^{14}N^{15}NO$ for the experiments at LURE to distinguish Nt^+ and Nc^+. The electric fields are applied so as to collect all energetic ions and separate three ions, $^{14}N^+$, $^{15}N^+$, and O^+, in the time-of-flight spectra. The errors in the measured TOF data originating from the deviation from the McLaren condition are corrected by a simulation. The resolution of angle is estimated to be 5°–10° for the ions with the kinetic energy of 10 eV.

III. RESULTS AND DISCUSSION

A. Nuclear motion at the $1s^{-1}3\pi$ resonances

The total ion yield spectra of N_2O around the N $1s \rightarrow 3\pi$ and O $1s \rightarrow 3\pi$ excitations are shown in Figs. 1(a) and 1(b), respectively. In Fig. 1(a), there are two resonance peaks at 401.0 and 404.6 eV, which are attributed to the Nt $1s \rightarrow 3\pi$ and Nc $1s \rightarrow 3\pi$ excitations, respectively.[17,28] In Fig. 1(b), there is a strong peak at 534.61 eV and a smaller peak at 536.64 eV, which are attributed to the O $1s \rightarrow 3\pi$ and O $1s \rightarrow 3s\sigma$ transitions, respectively. The vertical lines in Fig. 1 show the photon energies at which we probed the molecular geometry change following excitation.

The $1s^{-1}3\pi$ core-excited states of N_2O are split into A_1 and B_1 substates. In order to probe these substates separately, we select coincidence events corresponding to each substate as follows.[15,16] To probe the A_1 state, we selected the events in which the vector product of the two linear momenta of the Nt^+ and O^+ ions, $p(Nt^+) \times p(O^+)$, is perpendicular to the *E* vector (those having the angles between the vector product and the *E* vector larger than 70°) and $p(Nc^+)$ is at a certain angle with respect to *E*, depending on the Nt–O angle. In this

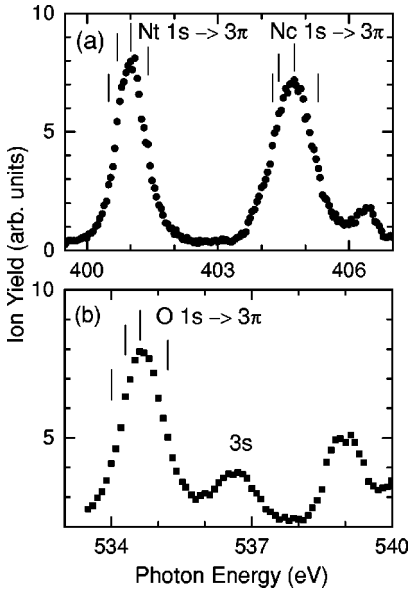

FIG. 1. Ion yield spectra of N_2O around (a) N $1s$ and (b) O $1s \rightarrow 3\pi$ excitations. Vertical lines show the photon energies where we probe the molecular geometry at the excited states.

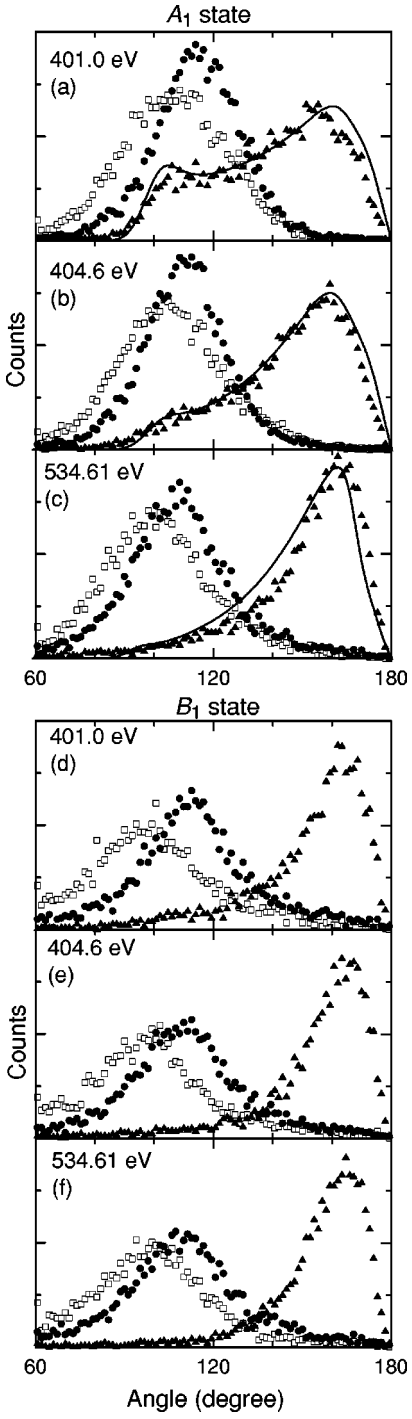

FIG. 2. Nt–O (closed triangles), Nc–Nt (open squares), and Nc–O (closed circles) correlation angle distributions of N_2O molecules in the A_1 [(a)–(c)] and B_1 [(d)–(f)] states. Panels (a) and (d) were measured at 401.0 eV ($Nt\,1s^{-1}3\pi$), (b) and (e) at 404.6 eV ($Nc\,1s^{-1}3\pi$), and (c) and (f) at 534.61 eV ($O\,1s^{-1}3\pi$). The solid curves show the calculated Nt–O angle distributions using the Coulomb explosion model.

way we selected the state in which the direction of the bending motion is parallel to E. To probe the excitation to the B_1 state, on the other hand, we selected the events in which $p(Nt^+) \times p(O^+)$ is parallel to the E vector (those having the angle between the vector product and the E vector less than 20°). In this way we selected the state in which the direction of the bending motion is perpendicular to E. The purities of the A_1 and B_1 states thus selected are estimated to be better than 96%.

We plot in Figs. 2(a)–2(f) the Nt–O (closed triangles), Nc–Nt (open squares), and Nc–O (closed circles) correlation angle distributions of N_2O molecules in the A_1 [(a)–(c)] and B_1 [(d)–(f)] states measured at 401.0 eV [$Nt\,1s^{-1}3\pi$, (a) and (d)], at 404.6 eV [$Nc\,1s^{-1}3\pi$, (b) and (e)], and at 534.61 eV [$O\,1s^{-1}3\pi$, (c) and (f)]. The Nt–O correlation angle means the angle between the linear momenta of the Nt^+ and O^+ ions detected in coincidence with the Nc^+ ion.

First we compare the Nt–O correlation angle distributions because it is easy, with those distributions, to see how the core-excited molecules are bent, the smaller angles meaning more bent geometry. The Nt–O correlation angle distributions of the B_1 states for the N $1s$ (d), Nc $1s$ (e), and O $1s$ (f) excitations have a similar symmetric profile with a peak at about 165°. These distributions are also similar to those obtained at wavelengths below the core-excitations and above the ionization thresholds. Although the N $1s$ ionized molecule is expected to be linear, the angular distribution results show that it is slightly bent. This is because the zero point bending vibration gives some initial momenta to the fragment ions in the linear geometry.[16] Since the Nt–O correlation angle distributions of the core-excited B_1 states have the same distribution as those for the core-ionized molecule, the molecule in the B_1 states may be concluded also to be linear. This result is consistent with the geometry of CO_2 in the B_1 states.[15,16]

On the other hand, the Nt–O correlation angle distributions of the A_1 states for the N $1s$ (a), Nc $1s$ (b), and O $1s$ (c) excitations extend down to about 90°. This difference in the Nt–O correlation angle distributions between the A_1 and B_1 states suggests that the core-excited N_2O molecules in the A_1 states are bent whereas those in the B_1 states are linear. The Nt–O correlation angle distribution for the $Nt\,1s^{-1}3\pi A_1$ state shows the intensity around 100° higher

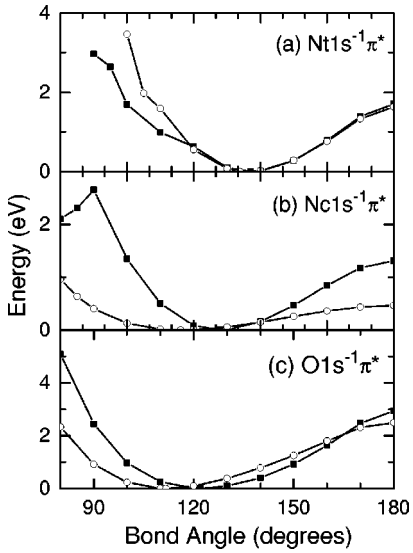

FIG. 3. Potential energy curves for the Nt, Nc, and O $1s^{-1}3\pi A_1$ states as a function of the bond angle calculated using a Hartree–Fock approximation. Closed squares and open circles indicate the potential energy curves for the bond lengths, the same as the initial ground state and the equilibrium bond lengths for the excited states, respectively.

than those for the Nc $1s^{-1}3\pi A_1$ or O $1s^{-1}3\pi A_1$ states, yielding that the molecule in the Nt $1s^{-1}3\pi A_1$ state is more bent than that in the Nc and O $1s^{-1}3\pi A_1$ states, a fact which is consistent with the result by LeBrun *et al.*[21] but inconsistent with the result by Adachi *et al.*[22]

The Nc–Nt and Nc–O correlation angle distributions have peaks at about 105° and 115°, respectively. This difference in the peak positions comes from asymmetric geometry of N_2O, i.e., when the molecule dissociates simultaneously into three fragments, the Nc^+ ion flies slightly towards the Nt^+ ion. The Nc–Nt and Nc–O correlation angle distributions have intensity at higher angles when the Nt–O correlation angle distributions have the intensity at smaller angles, as expected.

Now we discuss the Nt–O correlation angle distributions in detail. All the Nt–O correlation angle distributions for the A_1 state have a broad peak at ~167° and a long tail towards ~90°, as can be seen in Fig. 2. According to the Franck–Condon principle, the molecule is still linear immediately after excitation. Then the molecule starts to bend towards the turning point of the bending motion. The major peak at ~167° reflects the dissociation geometry after the Auger decay near the Franck–Condon point, where the excitation takes place. The long tail which extends to ~90° on the other hand reflects geometry of the dissociation that occurs on the way to the outer turning point in the A_1 state after the Auger decay. Two questions arise from these Nt–O correlation angle distributions. Although the outer turning points of the Nt, Nc, and O $1s^{-1}3\pi A_1$ states are expected to be about 100°, 90°, and 80°, respectively, from the Hartree–Fock calculation (see Fig. 3), the minima of these Nt–O correlation angle distributions are the same, about 90°. The Nt–O correlation angle could not be smaller than 117.2° due to the cutoff effect, which originates from the concept of simple repulsion force between the Nt^+ and O^+ fragment ions. The obtained angle distribution, however, does extend past 117.2° down to nearly 90°. The apparent discrepancy can be dissolved by considering the initial inhomogeneous charge distribution in the produced N_2O^{3+} ion and the momenta of the atoms originating from the bending motion of the molecular ion in the excited state.[15,16] The calculated initial charges on the atoms of the triply charged N_2O^{3+} ion are +1.26, +1.06, and +0.67 for the Nt, Nc, and O atoms, respectively, at the level of Hartree–Fock approximation. As the atoms depart, the charge on each atom approaches unity. These effects make the Nt–O correlation angle smaller. From the above discussion, one can find that the measured angle correlations do not coincide with the ejection angles when the dissociation takes place. They are affected by the Coulomb repulsion force after the dissociation. However, when the effect of Coulomb repulsion force after the dissociation is considered, one can still probe the molecular deformation.

Next we consider the different Nt–O correlation angle distributions among the Nt, Nc, and O $1s^{-1}3\pi A_1$ states. The nuclear motion in the core-excited molecules proceeds along a path on the potential energy surface within core-hole lifetime. Therefore the final molecular geometry of the core-excited states depends not only on the equilibrium bond angle but also on the potential energy surface and core-hole lifetime. Figure 3 shows the potential energy curves for the Nt, Nc, and O $1s^{-1}3\pi A_1$ states as a function of the bond angle calculated using a Hartree–Fock approximation. In the case of the Nt $1s$ and O $1s$ excited states, the potential energy curves for the initial bond lengths are very similar to those for the equilibrium bond lengths. However, the curve for the initial bond lengths is quite different from that for the equilibrium bond lengths in the case of Nc $1s$ excited state. This is because the bond lengths for the Nc $1s$ excited state change more extensively than those for the Nt $1s$ and O $1s$ excited states as shown in Table I, which lists the equilibrium

TABLE I. Calculated optical parameters for the core-excited states and ground state of $^{14}Nt^{15}NcO$.

Excited states	Bond length Nc–Nt (Å)	Bond length Nc–O (Å)	Equilibrium bond angle (°)	ν_2 (cm^{-1})
Nt*NcO	1.162	1.162	136.5	841.2
NtNc*O	1.125	1.784	116.1	348.9
NtNcO*	1.160	1.379	111.7	625.2
NtNcO	1.092	1.178	180.0	673.2
	1.13[a]	1.18[a]	180.0[a]	585[a]

[a]Experimental value (Ref. 32).

bond lengths as well as bond angles for the Nt, Nc, and $O\,1s^{-1}3\pi A_1$ states calculated using a Hartree–Fock approximation. The values are similar to those by Adachi *et al.*[22]

In order to investigate the effect of the potential energy surface and a core-hole lifetime, simulations for the Nt–O correlation angle distributions are performed based on a simple classical model.[29] In the simulation, the bending motion in the core-excited states is described classically. First, the molecule in the ground state with zero-point bending energy of 36.3 meV is excited to the core excited state. The bond angle of the molecule after the excitation is assumed to be the same as that before the excitation. If the excitation occurs at the bond angle of 180°, the molecule has the bending motion with the energy of 36.3 meV. On the other hand, if the excitation occurs at the minimum bond angle of zero-point bending motion, 176°, the excited molecule has no bending motion. The molecule is assumed to decay via Auger emission during the bending motion and then the triply charged parent ion N_2O^{3+} states to dissociate by Coulomb explosion producing fragment ions with the initial momenta gained from both the bending motion in the core-excited state and the zero-point bending motion in the ground state. The potential energy curves of the core-excited states for the initial bond lengths (solid squares) in Fig. 3 are used. We also take into account the stretching motion in the simulation because the kinematics of dissociation is strongly affected by the stretching mode. After dissociation, we calculate the classical trajectory of the fragment ions. In this calculation of the ion trajectory, charge clouds in a molecule are represented by single points at the atoms. The effect of the nonequivalent charge distribution on the three ions O^+, Nc^+, and Nt^+ in the early stage of the dissociation is of crucial importance in this model. Hsieh and Eland[30] introduced delocalization of charges as a charge exchange model. Here we treat delocalization of charges as a charge distribution. The initial charge distribution on the atoms of the triply charged N_2O^{3+} ion are $+1.26$, $+1.06$, and $+0.67$ for the Nt, Nc, and O atoms, respectively, by the Hartree–Fock approximation. The nonequivalent charge distribution is caused by the different electron affinity in the atoms in principle. The electron affinity of oxygen is larger than that of the nitrogen atom. When the bond length becomes larger than about 3 Å, the charge distributes equally. The repulsion force between the Nt and O atoms becomes smaller by this nonequivalent charge distribution, resulting that the Nt–O correlation angles are down to around 90°. The core-hole lifetime is assumed to be 5.5 fs for N 1*s* and 3.0 fs for O 1*s*, which is close to the core hole natural lifetime.

The results of the simulation, given in Fig. 2 by the solid curves, show reasonable agreements with the experimental results. The difference in the Nt–O correlation distribution between the Nt 1*s* and Nc 1*s* states can be mostly attributed to the difference in the depth of the potential energy surface. When the potential energy surface is steep, the molecule is forced to bend and then the probability for the molecule with a low Nt–O correlation angle becomes high in the short core-hole lifetime. The difference in the Nt–O correlation angle distribution between the Nt and $O\,1s^{-1}3\pi$ states can be mostly attributed to the difference in the core-hole lifetime, i.e., ~6 fs for N 1*s* and ~4 for O 1*s*. The $Nt\,1s^{-1}3\pi A_1$ state can survive longer in the core-excited state because the lifetime of the $N\,1s^{-1}$ hole is longer than that of the $O\,1s^{-1}$ hole.

The kinetic energy distributions of fragment ions are expected to be affected by the molecular deformation. Figure 4 shows the kinetic energy distributions of Nt^+, Nc^+, and O^+ in the A_1 [(a)–(c)] and B_1 [(d)–(f)] states measured at 401.0 eV [$Nt\,1s^{-1}3\pi$, (a) and (d)], at 404.6 eV [$Nc\,1s^{-1}3\pi$, (b) and (e)], and at 534.61 eV [$O\,1s^{-1}3\pi$, (c) and (f)], together with the calculated kinetic energy distributions by the Coulomb explosion model (solid curves). For the B_1 excited states, the kinetic energy distributions of Nt^+, Nc^+, and O^+ do not change with the photon energies and are identical to those for the core-ionized states (not shown here). This is because the core-excited molecules do not change their geometries by the bending motion. The Nc^+ ions for the A_1 excited states have kinetic energies larger than those for the B_1 excited states because the molecule is bent. The intensity of the Nc^+ kinetic energy distribution curve around 10 eV increases when the intensity of the Nt–O correlation angle distribution curve around 100° increases. The kinetic energy distributions of Nt^+ and O^+ ions have similar profiles. However, when the molecule is bent, the kinetic energy of Nt^+ and O^+ ions decrease because the Nc^+ ions have a large kinetic energy. The kinetic energy distributions of fragment ions directly depend on the geometry of the core-excited molecule just before dissociation. On the average, the Nc^+ ions at the Nt 1*s* excitation have larger kinetic energies than those at the Nc 1*s* excitation, which is consistent with the result by LeBrun *et al.*[21]

The calculated kinetic energy distributions by the Coulomb explosion model agree with the experimental distributions. If we neglect the stretching mode, the kinetic energy distributions of Nt^+ and O^+ do not agree between the calculation and the experiment. The kinetic energy distributions of Nc^+ strongly depend on the bending motion. The kinetic energy distributions depend on both the bending and the stretching motion.

B. Detuning effect at the $1s^{-1}3\pi$ resonances

When the excitation energy is detuned from the top of the resonance peak, how will the nuclear motion in the core-excited states be affected by it? Considering the Franck–Condon principle, the bond angle of the molecule excited to the A_1 state will become smaller with the decrease in the excitation energy. This difference in the initial geometry should affect the nuclear motion in the core-excited states. Figure 5 shows the Nt–O correlation angle distributions in the $Nt\,1s^{-1}3\pi A_1$ states measured at the photon energies of 400.5 (a), 401.0 (b, top of the resonance), and 401.4 eV (c). At the photon energy of 401.4 eV, the intensity at lower Nt–O correlation angles is seen to be decreased. On the other hand, the angle distributions at the photon energies of 400.5 and 401.0 eV are similar to each other. This fact suggests that the molecules excited with the photon energy higher than the peak of the resonance are less bent than that excited by the

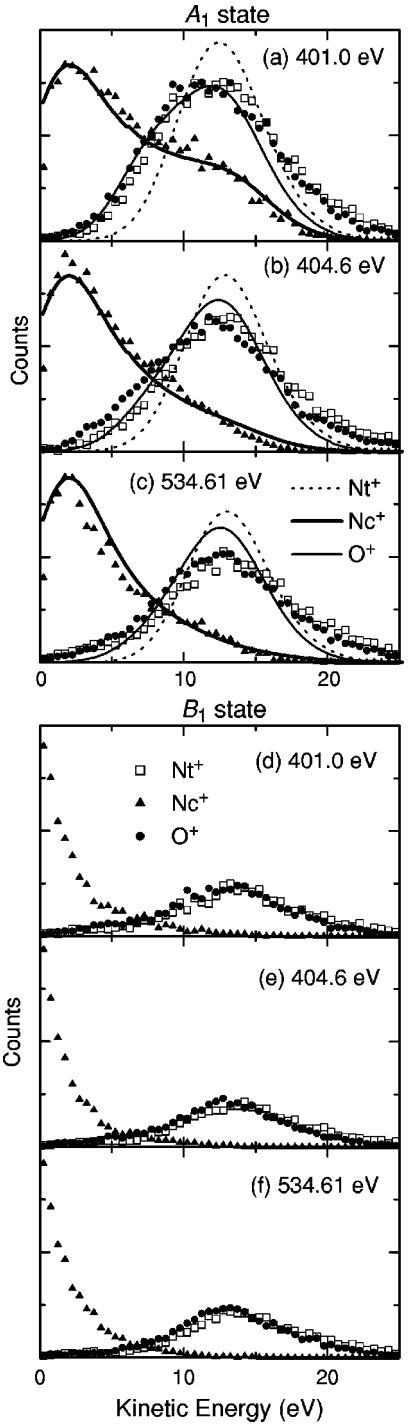

FIG. 4. Kinetic energy distributions of Nt^+ (open squares), Nc^+ (closed triangles), and O^+ (closed circles) ions from the triply charged N_2O molecules in the A_1 [(a)–(c)] and B_1 [(d)–(f)] core-excited states. Panels (a) and (d) were obtained at 401.0 eV ($Nt\,1s^{-1}3\pi$), (b) and (e) at 404.6 eV ($Nc\,1s^{-1}3\pi$), and (c) and (f) at 534.61 eV ($O\,1s^{-1}3\pi$). The dotted curves, thick curves, and thin curves in the A_1 [(a)–(c)] state are the kinetic energy distributions of Nt^+, Nc^+, and O^+ ions calculated from the Coulomb explosion model, respectively.

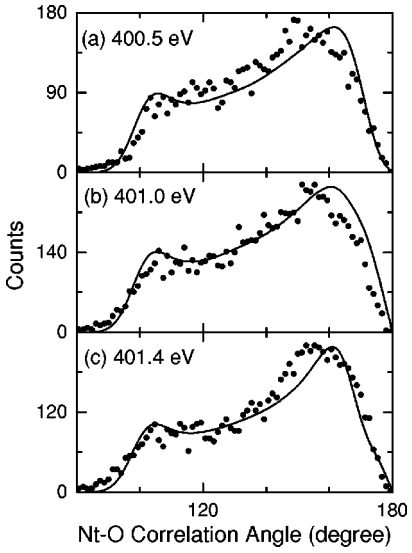

FIG. 5. Comparison among Nt–O correlation angle distributions of N_2O molecules in the $Nt\,1s^{-1}3\pi A_1$ states measured at 400.5 (a), 401.0 (b), and 401.4 eV (c). The dots are the experimental data and the curves are obtained by the calculation.

lower photon energy. This feature is consistent with the resonant Auger spectra from N_2O $Nt\,1s^{-1}3\pi$ to the $\tilde{X}\,^2\Pi$ ground state of N_2O^+.[31] The resonant Auger spectra have maximum around the binding energy of 15.7 eV, which are explained as the Auger electron ejected from the molecule at the bent geometry of the outer turning point. This maximum becomes very small when the excitation energy is larger than the peak of the resonance.

The slope of the potential energy surface determines the force for the nuclear motion in the core-excited states. The excitation at higher energies occurs in the larger bond angles, where the slope of the potential energy surface along the bending Q_2 coordinate is almost flat. In the case in which the molecule is excited with lower photon energies, the bond angle is smaller than that for higher photon energies and the slope of the potential energy surface is relatively steep. This difference in the slope changes the Nt–O correlation angle distributions. The similarity between the correlation angle distributions at the top and lower energies of the resonance suggests that the slopes of the core-excited potential surface are close to each other.

The Coulomb explosion model also reproduces this change in the Nt–O correlation angle distributions. We select the bond angle in the Franck–Condon region at the excitation near 180° for higher photon energy and 176° for lower photon energies. The solid curves in Fig. 5 show the calculated Nt–O correlation angle distributions for the three different excitation energies. Reasonably good agreement is seen between the calculated and experimental distributions. This good reproduction suggests that the nuclear motion in the core-excited states depends on the potential energy surface. A similar detuning effect is also seen in the O–O correlation angles for CO_2 at the $C\,1s^{-1}2p$ excitation.[15]

Finally, we discuss the branching ratios of the A_1 and B_1 excitations. In our previous work on CO_2,[15] the branching ratio of C/O $1s\rightarrow 2\pi_u\,A_1$ relative to the sum of C/O $1s\rightarrow 2\pi_u\,A_1$ and $1s\rightarrow 2\pi_u\,B_1$ was obtained as a function of detuning energy. The ratio of the A_1 excitation decreases with the increase in the excitation photon energy. This change of the branching ratio is explained by the fact that the lower branch of the RT splitting is the A_1 state with a bent

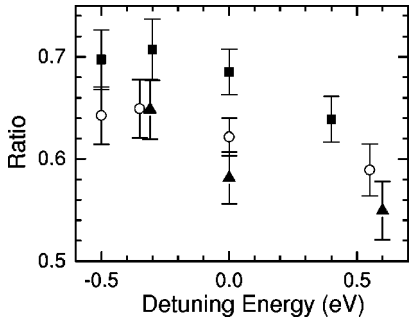

FIG. 6. The intensity ratios between A_1 and the sum of A_1 and B_1 for Nt $1s^{-1}3\pi$ (closed squares), Nc $1s^{-1}3\pi$ (open circles), and O $1s^{-1}3\pi$ (closed triangles) as a function of excitation energy. The energies in the top of the resonances are set to be zero in the excitation energy.

geometry. It is of great interest to examine the behavior of the branching ratios of the A_1 excitation in the case of N_2O because the potential energy surfaces of the core-excited states are quite different between N_2O and CO_2. This difference would affect the branching ratios. Figure 6 shows the intensity ratios between A_1 and the sum of A_1 and B_1 for the Nt $1s^{-1}3\pi$, Nc $1s^{-1}3\pi$, and O $1s^{-1}3\pi$ excitations as a function of excitation energy. The ratios for the excitation at the top of the resonances range from 0.58 to 0.7. These ratios are almost the same as those for the corresponding CO_2 transitions.[15] The ratios for all three different core excitations are seen to decrease with the increase in the excitation photon energy. These trends are also consistent with our previous results on CO_2.

IV. CONCLUSION

We have measured the linear momenta of the three fragment ions from inner-shell excited N_2O in coincidence by means of the ion momentum imaging technique. The nuclear motion in the core-excited state depends on the potential energy surface of the excited state and on the core-hole lifetime. The deep well in the potential energy surface of the Nt $1s^{-1}3\pi A_1$ state makes the molecules more bent than those in the Nc $1s^{-1}3\pi A_1$ state. When the excitation energy is increased within the resonance peak, the nuclear motion in the A_1 excited states becomes slower. On the other hand, the lower excitation energies in the resonance peak make the nuclear motion in the A_1 excited states faster. This result is explained from the Franck–Condon principle and the slope of the excited potential energy surface. The branching ratios of the A_1 excitation increase when the excitation energy decreases in the resonance. This change is smaller for the Nc $1s$ excitation. This is attributed to the shallower potential depth on the potential energy surface of the Nc $1s^{-1}3\pi A_1$ state.

ACKNOWLEDGMENTS

The experiments were carried out at Super-ACO and partly performed at the SPring-8 with the approval of JASRI. The authors are grateful to the staff of LURE and SPring-8 for their help. The work was supported in part by the Grant-in-Aid for Scientific Research (B) No. 12440169 from the Japan Society for the Promotion of Science (JSPS).

[1] M. Neeb, J. E. Rubensson, M. Biermann, and W. Eberhardt, J. Electron Spectrosc. Relat. Phenom. **67**, 261 (1994).
[2] U. Becker and A. Menzel, Nucl. Instrum. Methods Phys. Res. B **99**, 68 (1995).
[3] M. N. Piancastelli, M. Neeb, A. Kivimäki, B. Kempgens, H. M. Köppe, K. Maier, and A. M. Bradshaw, Phys. Rev. Lett. **77**, 4302 (1996).
[4] E. Kukk, H. Aksela, S. Aksela, F. Gel'mukhanov, H. Ågren, and S. Svensson, Phys. Rev. Lett. **76**, 3100 (1996).
[5] I. Nenner and P. Morin, in *VUV and Soft X-Ray Photoabsortion*, edited by U. Becker and D. A. Shirley (Plenum, New York, 1996), pp. 291–354.
[6] O. Björneholm, S. Sundin, S. Svensson, R. R. T. Marinho, A. Naves de Brito, F. Gel'mukhanov, and H. Ågren, Phys. Rev. Lett. **79**, 3150 (1997).
[7] P. Morin, M. Simon, C. Miron, N. Leclercq, E. Kukk, J. D. Bozek, and N. Berrah, Phys. Rev. A **61**, 050701(R) (2000).
[8] K. Ueda, J. Phys. B **36**, R1 (2003).
[9] M. Lavollée, Rev. Sci. Instrum. **70**, 2968 (1999).
[10] G. R. Wight and C. E. Brion, J. Electron Spectrosc. Relat. Phenom. **3**, 191 (1974).
[11] J. D. Bozek, N. Saito, and I. H. Suzuki, Phys. Rev. A **51**, 4563 (1995).
[12] J. Adachi, N. Kosugi, E. Shigemasa, and A. Yagishita, J. Phys. Chem. **100**, 19783 (1996).
[13] J. Adachi, N. Kosugi, E. Shigemasa, and A. Yagishita, J. Chem. Phys. **107**, 4919 (1997).
[14] E. Kukk, J. D. Bozek, and N. Berrah, Phys. Rev. A **62**, 032708 (2000).
[15] Y. Muramatsu, N. Saito, M. Lavollée *et al.* (unpublished).
[16] Y. Muramatsu, K. Ueda, N. Saito *et al.*, Phys. Rev. Lett. **88**, 133002 (2002).
[17] J. Adachi, N. Kosugi, E. Shigemasa, and A. Yagishita, J. Chem. Phys. **102**, 7369 (1995).
[18] See, for example, G. Herzberg, *Infrared and Raman Spectra of Polyatomic Molecules* (Van Nostrand, New York, 1973).
[19] N. Saito, K. Ueda, M. Simon *et al.*, Phys. Rev. A **62**, 042503 (2000).
[20] Y. Muramatsu, Y. Shimizu, H. Yoshida, K. Okada, N. Saito, I. Koyano, H. Tanaka, and K. Ueda, Chem. Phys. Lett. **330**, 91 (2000).
[21] T. LeBrun, M. Lavollée, M. Simon, and P. Morin, J. Chem. Phys. **98**, 2534 (1993).
[22] J. Adachi, N. Kosugi, E. Shigemasa, A. Yagishita, and P. A. Hatherly, J. Electron Spectrosc. Relat. Phenom. **79**, 491 (1996).
[23] M. Lavollée and V. Brems, J. Chem. Phys. **110**, 918 (1999).
[24] R. N. Zare, Mol. Photochem. **4**, 1 (1972).
[25] G. E. Busch and K. R. Wilson, J. Chem. Phys. **56**, 3638 (1972).
[26] H. Ohashi, E. Ishiguro, Y. Tamenori *et al.*, Nucl. Instrum. Methods Phys. Res. A **467–468**, 533 (2001).
[27] See http://www.roentdek.com for details of the detectors.
[28] K. C. Prince, L. Avaldi, M. Coreno, R. Camilloni, and M. de Simone, J. Phys. B **32**, 2551 (1999).
[29] U. Ankerhold, B. Esser, and F. von Busch, J. Phys. B **30**, 1207 (1997).
[30] S. Hsieh and J. H. D. Eland, J. Chem. Phys. **103**, 1006 (1995).
[31] C. Miron, M. Simon, P. Morin *et al.*, J. Chem. Phys. **115**, 864 (2001).
[32] T. Shimanouchi, *Tables of Molecular Vibrational Frequencies Consolidated Volume I* (National Bureau of Standards, Washington, DC, 1972).